American Mineralogist, Volume 93, pages 1393–1403, 2008

Pressure-induced over-hydration and water ordering in gismondine: A synchrotron powder diffraction study

SILVIA ORI,[1] SIMONA QUARTIERI,[2,*] GIOVANNA VEZZALINI,[1] AND VLADIMIR DMITRIEV[3]

[1]Dipartimento di Scienze della Terra, Università di Modena e Reggio Emilia, Via S. Eufemia 19, 41100 Modena, Italy
[2]Dipartimento di Scienze della Terra, Università di Messina, Salita Sperone 31, 98166 Messina S. Agata, Italy
[3]Swiss-Norwegian Beam Lines at ESRF, BP220, 38043 Grenoble Cedex, France

ABSTRACT

This paper reports the results of an in situ HP synchrotron X-ray powder diffraction investigation on the natural zeolite gismondine (ideal chemical formula $Ca_4Al_8Si_8O_{32}\cdot 16H_2O$, space group $P2_1/c$). The study was performed from P_{amb} to 7.9 GPa, and upon decompression, using methanol:ethanol:water (16:3:1) mixture (m.e.w.) as a nominally penetrating hydrostatic *P*-transmitting medium. No complete X-ray amorphization is observed up to the highest investigated pressure, and the original unit-cell parameters are almost completely recovered upon decompression. From 0.6 GPa, the water content is slightly higher than at ambient pressure, as a result of a moderate over-hydration. Moreover, at about 2 GPa, a significant water molecule system re-arrangement occurs, characterized by an ordering of part of the water molecules from four partially occupied sites to only two fully occupied ones. The over-hydration, but not the water ordering, is substantially irreversible upon pressure release. The Rietveld structural refinements of the powder patterns converged successfully up to 2.8 GPa; above this pressure, a phase transition to triclinic symmetry was observed and only the unit-cell parameters were refined. The comparison of the overall cell volume reductions and of the bulk modula of gismondine compressed between P_{amb} and 7.9 GPa in m.e.w. and in silicone oil, reveals that this is the unique zeolite with a higher compressibility in penetrating vs. non-penetrating *P*-transmitting media. This is ascribed to the re-organization of the water molecule system upon compression in m.e.w., which leaves a larger free volume inside the pores with respect to the phase compressed in silicone oil.

Keywords: Zeolite, gismondine, high pressure, compressibility, over-hydration, phase transition, crystal structure, synchrotron XRPD data

INTRODUCTION

High-pressure (HP) structural studies on zeolites compressed in aqueous media have recently attracted great interest in the so-called pressure-induced hydration (PIH) phenomenon (Lee et al. 2004a), which is characterized by the penetration of additional water molecules into the zeolite channels. This over-hydration, and the consequent structural modifications, can in principle significantly modify the zeolite properties, opening possible new scenarios for their industrial applications.

The HP studies performed up to now on zeolites using "pore penetrating" *P*-transmitting media are summarized in Table 1; in the last column of this table the main structural changes induced by compression are noted. These experiments show that zeolites can undergo the following different effects: (1) HP-induced structural modifications, without over-hydration; (2) PIH, based on increasing occupancy of already existing water sites; and/or (3) PIH, accompanied by the onset of new water sites (see Ori 2008 for a review).

In the case of analcime, investigated by Gatta et al. (2006) using a (16:3:1) methanol:ethanol:water mixture (m.e.w.), a full structural refinement was performed, and no evidence of PIH was observed. The same result was also obtained for the fibrous zeolites edingtonite and thomsonite (Lee et al. 2004a) and mordenite (Gatta and Lee 2006), again studied employing m.e.w. In the last two investigations, the HP diffraction data were not good enough to allow detailed structural refinements, but in any case the authors rule out PIH on the basis of the analysis of the unit-cell HP modifications. In edingtonite (Gatta et al. 2004a, 2004b), an increase of the occupancy factors of the water molecule sites was observed upon compression. However, since the related errors were of the same order of magnitude as the observed variations, the authors assumed the absence of a true PIH effect.

Several experiments performed compressing zeolites in hydrous ambient (Hazen 1983; Hazen and Finger 1984; Lee et al. 2001b, 2002a) suggest the possible entry of water molecules into the cavities only on the basis of a positive volume discontinuity, without the support of detailed structural data (see Table 1 for further information). Zeolite A was investigated both with distilled water and H_2O-bearing methanol:ethanol (4:1) mixture (Hazen 1983; Hazen and Finger 1984). The volume response to pressure was considered dependent on the different *P*-transmitting media. As a consequence, the authors suggested that the different observed volume discontinuities could derive from sorption of water and/or alcohol molecules from the transmitting media. A similar interpretation of the *P*-induced cell-volume variations was proposed by Lee et al. (2001b) for NaCs, Cd, Li-RHO zeo-

* E-mail: simona.quartieri@unimore.it

TABLE 1. Schematic summary of the results reported in literature for HP experiments on zeolites using penetrating *P*-transmitting media and performed by X-ray powder diffraction (XRPD) or single-crystal X-ray diffraction (SC-XRD)

	P_{max} (GPa)	*P*-transmitting medium	XRPD	SC-XRD	Refinement of only cell parameters
Natrolite (Lee et al 2001a)	5	m.e.w.* (16:3:1)	x		
Tetranatrolite (Lee et al. 2006)	~7	m.e.w. (16:3:1)	x		
Synthetic K-GaSi- natrolite (Lee et al. 2002b)	~2	m.e.w. (16:3:1)		x	
Mesolite (Lee et al. 2002a)	5	m.e.w. (16:3:1)	x		x
Scolecite (Likhacheva et al. 2006)	2	m.e.w. (4:1:1)	x		
Edingtonite (Gatta et al. 2004a, 2004b)	~7	m.e.w. (16:3:1)		x	
Edingtonite (Lee et al. 2004a)	6	m.e.w. (16:3:1)	x		x
Thomsonite (Lee et al. 2004a)	6	m.e.w. (16:3:1)	x		x
Thomsonite (Likhacheva et al. 2007)	3	ethanol-water(1:3)	x		
Zeolite Na-A (Hazen 1983; Hazen and Finger 1984)	4	methanol-ethanol (4:1); distilled water		x	x
Zeolite Y (Colligan et al. 2004)	8	m.e.w. (16:3:1)	x		
Zeolite X (Colligan et al. 2004)	5	m.e.w. (16:3:1)	x		x
NaCs-; Cd-; Li-RHO (Lee et al. 2001b)	3	m.e.w. (16:3:1)	x		x
Partially dehydrated laumontite (Lee et al. 2004b)	~7	m.e.w. (16:3:1)	x		
Mordenite (Gatta and Lee 2006)	~6	m.e.w. (16:3:1)	x		x
Analcime (Gatta et al. 2006)	~7	m.e.w. (16:3:1)		x	
Gismondine (this work)	~8	m.e.w. (16:3:1)	x		

* Methanol-ethanol-water.

lites. Lee et al. (2002a) proposed a *P*-induced disordering of the extra-framework cations Na and Ca to interpret the HP unit cell of mesolite, while a *P*-induced partial amorphization was observed by the same authors in scolecite. Both phenomena were ascribed to the probable (but not ascertained) entering of additional water molecules into the respective nano-channels.

Until now, certain signs of water sorption from an alcohol-based *P*-transmitting medium into zeolite pores were evidenced by detailed structural refinements of the following zeolites: (1) natrolite and related phases (tetranatrolite and the synthetic potassium gallosilicate natrolite) (Lee et al. 2001a, 2002a, 2002b, 2006; Colligan et al. 2005; Seryotkin et al. 2005); (2) partially dehydrated laumontite (Lee et al. 2004b); (3) scolecite (Likhacheva et al. 2006); and (4) thomsonite (Likhacheva et al. 2007). For natrolite and its analogues, the observed *P*-induced volume expansion was demonstrated to occur through the selective sorption of water molecules from the hydrostatic pressure fluid (m.e.w.), giving rise to new additional water positions in the framework channels (Lee et al. 2001a, 2002a, 2002b; Colligan et al. 2005; Seryotkin et al. 2005). A cell-volume increase between P_{amb} and 0.2 GPa was also observed for a partially dehydrated laumontite, due to an increase of the water content from about 12 to 18 molecules per unit cell (Lee et al. 2004b). Very recently the HP behaviors of scolecite and thomsonite have been investigated using water-rich mixtures of ethanol and water (3:1 to 1:3; Likhacheva et al. 2006, 2007). The high-hydrated scolecite is expanded by 5% as compared with the original scolecite, due to the increase of zeolitic water from 3 to 4.6 molecules pfu (Likhacheva et al. 2006). The transition to an over-hydrated state was attested in thomsonite at 2 GPa, proved by the appearance of a new half-occupied water position (Likhacheva et al. 2007). This result, in contrast with that obtained by Lee et al. (2004a) using m.e.w., demonstrates that the PIH effect, at least for fibrous zeolites, strongly depends on the partial water pressure in the compressing medium (Likhacheva et al. 2007).

Finally, for the purely siliceous zeolite Y, Colligan et al. (2004) attested the progressive filling of six different partially occupied water sites, highlighting, however, the undefined nature of the molecules (water or methanol) entering the zeolite pores. A similar compressibility behavior was also observed for synthetic zeolite Na-X in preliminary HP experiments in aqueous medium (Colligan et al. 2004).

In this paper, we present the results of a HP investigation of gismondine in aqueous medium. The only previous study on the HP stability of gismondine was performed by our group (Betti et al. 2007) using in situ synchrotron X-ray powder diffraction (XRPD) and Car-Parinello molecular dynamics simulations. Gismondine was investigated from P_{amb} to 7.4 GPa, and upon decompression, using silicone oil (s.o.) as a non-penetrating *P*-transmitting medium. No pressure-induced amorphization occurred and the cell-volume decrease was ~8%. We observed a decrease in the degree of monoclicity of the structure and a trend toward tetragonality with increasing pressure. In any case, the structure preserved its monoclinic lattice up to 7.4 GPa. At this pressure, the initial growth of a new phase was observed. The molecular dynamics simulations revealed that the deformation mechanism is linked to the distortion of the "double crankshaft" chains elongating in the *a* and *c* directions, similar to the deformations observed during dehydration under vacuum (Vezzalini et al. 1993). Moreover, upon compression, the Ca coordination number increased and the water molecules organized themselves in a slightly different supra-molecular arrangement.

The presence of several partially occupied water sites in gismondine channels suggested the possibility that these sites could undergo over-hydration/reorganization upon compression in an aqueous medium, and hence a new HP investigation was undertaken, compressing gismondine in m.e.w.

The aims of the present work are (1) to investigate the elastic behavior and the HP-structural evolution of gismondine by means of in situ synchrotron XRPD using a penetrating *P*-transmitting medium; (2) to verify the capacity of gismondine to host additional water molecules inside its structure; (3) to compare our results with those obtained using s.o. as a non-penetrating *P*-transmitting medium (Betti et al. 2007), to identify the influence of the different media on the compressibility and on the HP deformation mechanisms of this zeolite.

TABLE 1.—*EXTENDED*

Complete structural refinement	HP induced effects
x	PIH with water-content doubling ($P > 1.5$ GPa)
x	PIH with tetragonal-monoclinic phase transition with positive V discontinuities ($P > 0.2$ GPa), and monoclinic-tetragonal phase transition with negative V discontinuities (>3 GPa)
x	Irreversible PIH with water content doubling ($P > 1.2$ GPa)
	P-induced cation disordering with positive V discontinuity (1.7 GPa)
x	PIH with new water sites (1.2 GPa)
x	Regular volume decrease
	Regular volume decrease
	Regular volume decrease
x	PIH with one additional half occupied water site (2 GPa)
	Negative V discontinuities in methanol-ethanol (0.2–0.3 GPa); in water regular volume decrease
x	PIH with water (or alcohol) content increasing; positive V discontinuity ($P > 4$ GPa)
	Positive V discontinuity
	Centric cubic-acentric cubic phase transition ($P > 0.2$GPa)
x (up to 2.4 GPa)	Re-hydration, new water sites, water migration (0.2 GPa); supercell ($P > 3$ GPa)
	Regular volume decrease
x	Cubic-triclinic phase transition (1 GPa)
x (up to 2.8 GPa)	Moderate PIH, water site ordering (1.9 GPa)

GISMONDINE CRYSTAL STRUCTURE

Gismondine (ideal chemical formula $Ca_4Al_8Si_8O_{32}\cdot 16H_2O$, space group $P2_1/c$) is quite a rare zeolite. It is described as the calcium ordered member of the gismondine group (gismondine, amicite, garronite, gobbinsite). Its framework topology (GIS, after Baerlocher et al. 2001) is also shared by several synthetic phases, among which is zeolite Na-P (Håkansson et al.1990; Adams et al. 1997). The gismondine crystal structure was originally determined by Fischer and Schramm (1971) and then refined by Rinaldi and Vezzalini (1985) and Artioli et al. (1986).

The gismondine framework is formed by intersecting ribbons of 4-membered rings of tetrahedra running in the *a* and *c* directions (Fig. 1), laterally linked to form two sets of channels delimited by quite regular 8-membered rings running parallel to [100] and [001]. The maximum symmetry of GIS topology $I4_1/amd$ is lowered in gismondine to the space group $P2_1/c$ by the distribution of the extra-framework cations Ca and by the Al ordering on two preferred tetrahedra (Al1 and Al2). Among the extraframework sites, one is fully occupied by calcium and seven by water molecules. Three of these water sites (W1, W2, W3) are fully occupied, while the others (W4, W5, W6, W7) show partial occupancies. In particular, the pairs of sites W4-W5, and W6-W7 are too near each other to be simultaneously occupied. The Ca atom is bonded to two framework O atoms (O4 and O8) and to all the seven water molecules.

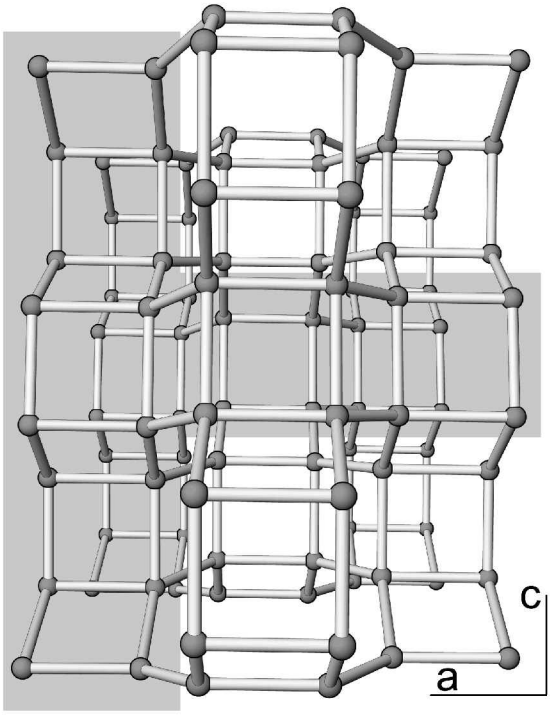

FIGURE 1. Skeletal representation of the gismondine framework viewed down the [010] direction. The alignment of the "double crankshaft" chains along *a* and *c* directions are evidenced by shading.

EXPERIMENTAL METHODS AND DATA ANALYSIS

The gismondine sample used in this study comes from Ballyclare (Ireland) [chemical formula: $K_{0.03}Na_{0.22}Ca_{3.77}Al_{7.53}Si_{8.41}O_{32}\cdot 17.76H_2O$, space group $P2_1/c$ (Vezzalini and Oberti 1984)]. The unit-cell parameters determined at ambient conditions on the powder inside the diamond anvil cell (DAC) are $a = 10.0155(5)$ Å, $b = 10.6051(5)$ Å, $c = 9.8277(5)$ Å, $\beta = 92.409(3)°$, and $V = 1042.9(1)$ Å^3.

The HP XRPD experiments were performed at the SNBL1 (BM01a) beamline at European Synchrotron Radiation Facility (ESRF) with fixed wavelength of 0.7 Å, using a modified Merril-Bassett DAC (Miletich et al. 2000) and a mixture of methanol-ethanol-water in the proportion 16:3:1 as hydrostatic *P*-transmitting medium. The pressure was measured using the ruby fluorescence method (Forman et al. 1972) on the non-linear hydrostatic pressure scale (Mao et al. 1986). The estimated error in the pressure values is 0.1 GPa. A MAR345 detector (pixel dimension 150 μm) was used at a fixed distance of 230 mm from the sample; the exposure time was 300 s for all pressures. One-dimensional diffraction patterns were obtained in the 2θ range 0–47° by integrating the two dimensional images with the program FIT2D (Hammersley et al. 1996) and are reported in Figure 2.

The experiments were performed from P_{amb} up to 7.9 GPa, with ΔP increments of about 0.1–0.6 GPa. The sample was equilibrated for about 30 min at each measured pressure. Three other patterns were collected upon decompression, from the highest pressure to P_{amb}. In all, 29 spectra were collected.

The data analysis was performed in the whole studied *P* range, adopting different strategies in the two ranges P_{amb}–2.8 GPa and 3.3–7.9 GPa. Whereas complete Rietveld structural refinements were performed in the first *P* interval, above 2.8 GPa a *P*-induced symmetry lowering was observed, and only the unit-cell values were extracted from the diffraction patterns.

The Rietveld profile fitting of 13 patterns in the range P_{amb}–2.8 GPa and of one pattern collected at P_{amb} after pressure release [hereafter labeled P_{amb}(rev)] was

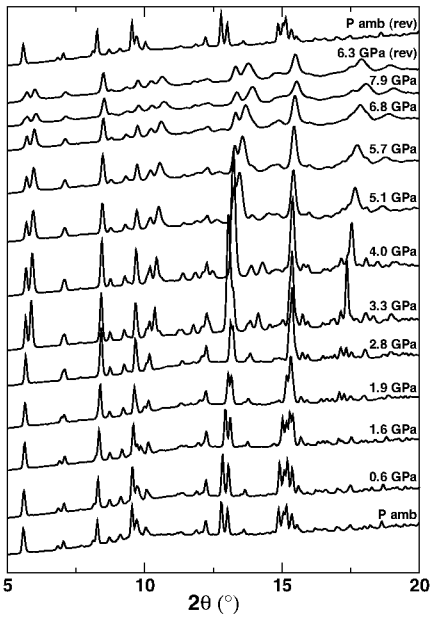

FIGURE 2. Selected integrated powder patterns of gismondine as a function of pressure, reported in the 2θ range 4–20°. The powder patterns at the top of the figure were collected during decompression.

performed in the 2θ range 3–34.7° using of the GSAS package (Larson and Von Dreele 1996) with the EXPGUI (Toby 2001) interface. The atomic coordinates of the adopted structural model are from Rinaldi and Vezzalini (1985). The experimental intensities were corrected for the absorption of the Be backing plates. The background curves were fitted by a Chebyshev polynomial with an average of 11 coefficients in the 2θ range 3–10.5° and 24 coefficients for the range 10.5–34.7°. The pseudo-Voigt profile function proposed by Thomson et al. (1987) and cut-off of the peak intensity were applied.

Soft-restraints were applied to the T-O distances [Si-O = 1.62(2); Al-O = 1.74(2)] and gradually released after the initial stages of refinement, up to a final weight equal to 50. The isotropic displacement parameters were constrained in the following way: the same value for all tetrahedral cations [as suggested by the results of the single-crystal structure refinement of gismondine at ambient conditions (Rinaldi and Vezzalini 1985)], a second value for all framework O atoms, a third one for the Ca extra-framework cation, and a final one for the water molecules. The unit-cell parameters of gismondine were allowed to vary for all refinement cycles. In the final cycles, only the atomic coordinates and the occupancy factors of all the atoms were refined. The Ca and the water molecules W1, W2, W3 sites were shown to be fully occupied in all the refinements. From P_{amb} to 1.6 GPa and at P_{amb}(rev) the occupancy factors of W4 and W5 were constrained by each other to sum to 100%, because the distance between them was too short to allow their simultaneous presence. Occupancy factors of W6 and W7 were allowed to vary from P_{amb} to 1.0 GPa and at P_{amb}(rev); from 1.1 to 1.6 GPa they were constrained to sum 100%, again due to their small separation. In the P range 1.9–2.8 GPa, W4 and W6 progressively disappeared, while W5 and W7 became fully occupied. Scattering factors for neutral atoms (Cromer and Waber 1974) were used for all species (Si, Al, O-framework/water Ca).

The structure of Rinaldi and Vezzalini (1985) was used as the starting model for the refinement at P_{amb}, and the same labeling was assumed. As a result of the Rietveld refinement, the total electron number obtained for the water molecules was 152, in good agreement with the chemical formula (Vezzalini and Oberti 1984).

The Rietveld refinement of the powder patterns converged successfully up to 2.8 GPa; at 3.3 GPa some new peaks, not indexable in the monoclinic space group, appeared, indicating the onset of a new phase. Above this pressure, the failure of the structural refinement reinforced the hypothesis of a phase transition. At 3.3 GPa, the unit-cell symmetry indicated by the TREOR program (Werner et al. 1985)—used for indexing and space group determination—was $P\bar{1}$. Because of the consequent increase of the number of independent parameters and of the inadequate quality of the powder patterns, any attempt at structural refinement of the triclinic phase failed and only the unit-cell parameters were extracted from the diffraction data using the Le Bail whole pattern fitting by GSAS package (Le Bail et al. 1988; Larson and Von Dreele 1996). During these refinements the background was graphically fitted, and not refined, to avoid divergence effects.

The refined cell parameters as a function of pressure are reported in Table 2 and Figure 3.

The P-induced structural modifications of monoclinic gismondine were studied on the basis of 14 structural refinements at P_{amb}, 0.1, 0.2, 0.4, 0.6, 0.8, 1.0, 1.1, 1.6, 1.9, 2.2, 2.4, and 2.8 GPa and at ambient conditions after pressure release [P_{amb} (rev)]. Tables 3–6 report the refinement details and the structural data for the selected refinements at P_{amb}, 1.6, 1.9 GPa, and at P_{amb}(rev). Figures 4–5

TABLE 2. Unit-cell constants of gismondine at the investigated pressures

P (GPa)	a (Å)	b (Å)	c (Å)	α (°)	β (°)	γ (°)	V (Å^3)
P_{amb}	10.0155(5)	10.6051(5)	9.8277(5)	–	92.409(3)	–	1042.9(1)
0.1	10.0157(4)	10.6051(4)	9.8279(4)	–	92.414(3)	–	1043.0(1)
0.2	10.0110(4)	10.6059(5)	9.8239(4)	–	92.408(3)	–	1042.1(1)
0.4	9.9967(5)	10.6030(5)	9.8142(5)	–	92.415(3)	–	1039.3(1)
0.6	9.9790(4)	10.6004(5)	9.8013(4)	–	92.396(3)	–	1035.9(1)
0.8	9.9647(5)	10.5982(5)	9.7924(5)	–	92.385(3)	–	1033.2(1)
1.0	9.9480(4)	10.5976(5)	9.7826(4)	–	92.355(3)	–	1030.5(1)
1.1	9.9312(9)	10.593(1)	9.7715(9)	–	92.320(6)	–	1027.2(3)
1.6	9.8917(6)	10.5948(7)	9.7482(6)	–	92.200(4)	–	1020.9(2)
1.9	9.7975(9)	10.626(1)	9.6977(8)	–	91.225(7)	–	1009.4(2)
2.2	9.781(1)	10.625(1)	9.688(1)	–	91.134(9)	–	1006.5(3)
2.4	9.754(1)	10.620(1)	9.672(1)	–	91.027(8)	–	1001.8(3)
2.8	9.728(1)	10.612(1)	9.655(1)	–	90.938(7)	–	996.6(3)
3.3	9.689(1)	10.604(2)	9.638(1)	89.22(2)	91.611(9)	92.54(1)	988.8(4)
3.8	9.671(1)	10.596(1)	9.607(2)	89.06(1)	91.571(9)	92.81(1)	982.8(3)
4.0	9.664(1)	10.586(2)	9.591(2)	89.03(2)	91.543(9)	92.92(1)	979.5(4)
4.3	9.672(2)	10.569(2)	9.577(3)	88.65(2)	91.54(2)	93.62(2)	976.4(6)
4.6	9.696(2)	10.562(2)	9.553(2)	88.19(2)	91.39(1)	93.87(1)	975.6(5)
4.7	9.682(2)	10.553(2)	9.533(2)	88.15(1)	90.37(1)	93.89(1)	971.3(5)
5.1	9.672(2)	10.546(2)	9.517(1)	88.06(1)	90.28(2)	93.98(1)	967.9(4)
5.5	9.664(2)	10.541(2)	9.503(2)	88.01(1)	90.22(2)	94.04(1)	965.1(5)
5.7	9.659(2)	10.535(2)	9.491(1)	87.97(1)	90.15(2)	94.11(1)	962.7(4)
6.5	9.632(2)	10.516(3)	9.448(2)	87.85(1)	90.07(2)	94.29(1)	953.6(5)
6.8	9.604(2)	10.485(3)	9.424(2)	87.77(1)	89.92(2)	94.25(1)	945.6(6)
7.4	9.576(3)	10.470(3)	9.372(3)	87.63(2)	89.98(2)	94.41(2)	936.1(6)
7.9	9.547(2)	10.447(2)	9.347(2)	87.62(1)	89.93(2)	94.40(1)	928.6(5)
6.3(rev)	9.632(3)	10.512(3)	9.436(2)	87.68(1)	90.04(2)	94.33(2)	951.9(6)
3.5(rev)	9.683(2)	10.598(3)	9.615(2)	89.12(2)	91.59(1)	92.69(2)	985.1(5)
P_{amb}(rev)	10.0264(8)	10.6094(8)	9.8377(7)	–	92.369(5)	–	1045.6(2)

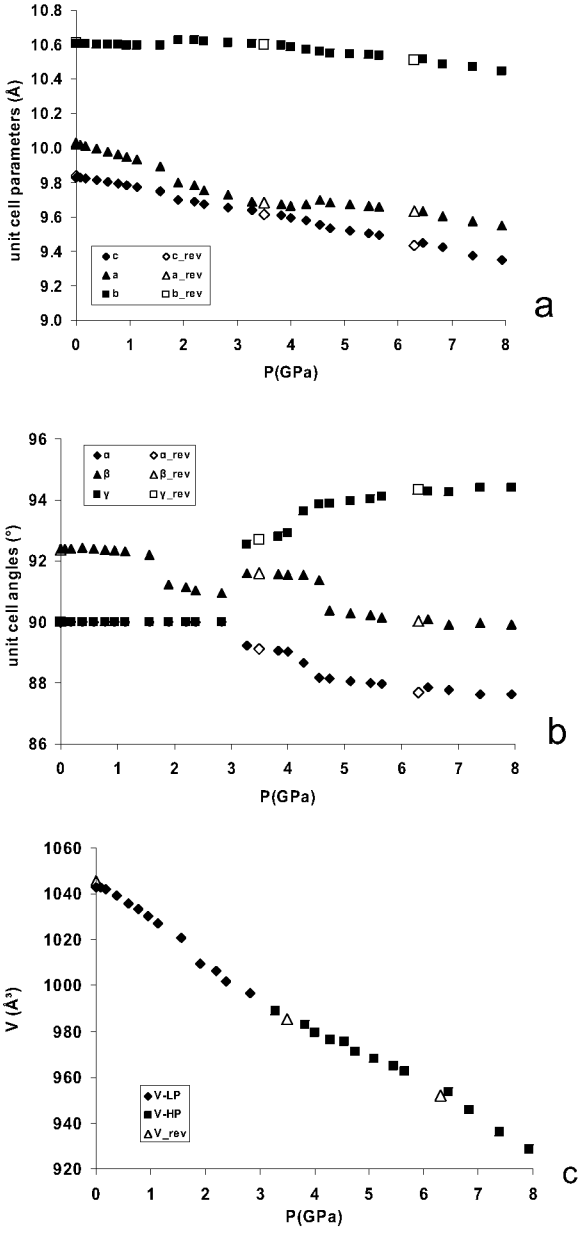

FIGURE 3. Variation of gismondine lattice parameters as a function of pressure: (**a**) unit-cell axes; (**b**) unit-cell angles; (**c**) unit-cell volume. The errors associated with the cell parameters are smaller than the symbol size. Open symbols are associated with the lattice values measured during decompression.

show the projections of the monoclinic gismondine structure at P_{amb}, 1.9 GPa, and P_{amb}(rev). The projections of the structure at 1.6 GPa are not drawn, being very similar to those at P_{amb}.

RESULTS AND DISCUSSION

From the inspection of Figure 2, which shows selected experimental powder patterns of gismondine as a function of pressure, it is evident that the peak intensities generally decrease and the peak profiles become broader with increasing pressure. These effects can be due to several factors, such as an increase in the long range structural disorder, and the presence of texture effects.

TABLE 3. Details of the structural refinements of monoclinic gismondine at selected pressures

	P_{amb}	1.6 GPa	1.9 GPa	P_{amb}(rev)
a (Å)	10.0155(5)	9.8917(6)	9.7975(9)	10.0264(8)
b (Å)	10.6051(5)	10.5948(7)	10.626(1)	10.6094(8)
c (Å)	9.8277(5)	9.7482(6)	9.6977(8)	9.8377(7)
α (°)	90.0	90.0	90.0	90.0
β (°)	92.409(3)	92.200(4)	91.225(7)	92.369(5)
γ (°)	90.0	90.0	90.0	90.0
Cell volume (Å³)	1042.9(1)	1020.9(2)	1009.4(2)	1045.6(2)
R_p (%)	0.34	0.47	0.51	0.36
R_{wp} (%)	0.44	0.67	0.71	0.52
$R_{F^{**}2}$ (%)	8.69	6.36	8.39	8.54
χ^2	0.482	2.486	2.753	1.601
No. of variables	109	107	99	109
No. of observations	1120	1106	1106	1108
No. of reflections	679	692	679	693

However, HP XRPD data demonstrate that gismondine does not undergo complete amorphization up to the highest investigated pressure. Moreover, the ambient pressure pattern features are almost completely recovered upon decompression. These results are in agreement with those of Betti et al. (2007), even if, in that case, reversibility of gismondine *P*-induced deformations was ascertained only from 7.4 to 4 GPa.

Figure 3 and Table 2 show several discontinuities in the cell parameters *P*-dependences. In particular, the trends of the unit-cell axes and angles allow to single out the following six *P* ranges: (1) P_{amb}–1.6 GPa; (2) 1.9–2.8 GPa; (3) 3.3–4.0 GPa; (4) 4.3–4.7 GPa; (5) 5.1–5.7 GPa; and (6) 6.5–7.9 GPa. The discontinuity at about 3.3 GPa corresponds to the monoclinic-triclinic transition, which is also clearly visible in the sequence of powder patterns (Fig. 2). Another clear discontinuity occurs at about 2 GPa, where all the cell parameters undergo an abrupt, even if small, change. In particular, a substantial decrease of β angle is observed. This trend is similar to that found by Betti et al. (2007), who report a comparable lowering in the degree of monoclinicity for gismondine in s.o. The discontinuities in the cell parameters occurring after the monoclinic-triclinic phase transition could not be interpreted from the structural point of view, due to the impossibility of performing structural refinements on triclinic gismondine. This study is now in progress by means of a combined experimental-computational approach, based on ab initio molecular dynamics simulations of the triclinic gismondine as a function of pressure (in preparation).

Concerning the unit-cell volume, a reduction of about 4 and 7% is observed for the monoclinic and the triclinic phases, respectively, corresponding to an overall reduction of about 11% in the whole investigated *P* range. The total reductions of unit-cell axes are about 5, 2, and 5% for *a*, *b*, and *c*, respectively. The α and β unit-cell angles both decrease by about 3%, while γ increases by about 5%.

Based on the unit-cell parameter values measured after decompression to P_{amb}, we can assume that the monoclinic to triclinic phase transition is reversible. No appreciable hysteresis effects are observed, and the ambient unit-cell parameters are almost completely recovered.

P-INDUCED STRUCTURAL DEFORMATIONS IN MONOCLINIC GISMONDINE

Framework. The framework atomic positions refined in this study for the structure at P_{amb} are in excellent agreement with

TABLE 4. Refined atomic positions and displacement parameters (Å²) of monoclinic gismondine at selected pressures

	P_{amb}					1.6 GPa				
	x/a	y/b	z/c	Occ.	U_{iso}	x/a	y/b	z/c	Occ.	U_{iso}
Si1	0.4110(7)	0.1088(9)	0.1791(9)	1	0.015(1)	0.412(1)	0.112(1)	0.183(1)	1	0.026(2)
Si2	0.9101(8)	0.870(1)	0.1618(8)	1	0.015(1)	0.909(1)	0.866(1)	0.163(1)	1	0.026(2)
Al1	0.0987(7)	0.1136(9)	0.1671(8)	1	0.015(1)	0.095(1)	0.113(1)	0.168(1)	1	0.026(2)
Al2	0.5917(8)	0.8652(9)	0.1514(8)	1	0.015(1)	0.591(1)	0.863(1)	0.151(1)	1	0.026(2)
O1	0.072(2)	0.159(1)	0.9981(8)	1	0.005(2)	0.071(2)	0.160(2)	0.998(1)	1	0.016(2)
O2	0.2608(6)	0.067(1)	0.215(1)	1	0.005(2)	0.260(1)	0.072(2)	0.221(2)	1	0.016(2)
O3	0.435(1)	0.151(2)	0.0237(8)	1	0.005(2)	0.436(2)	0.151(2)	0.026(1)	1	0.016(2)
O4	0.2430(7)	0.401(2)	0.302(1)	1	0.005(2)	0.243(1)	0.404(2)	0.298(2)	1	0.016(2)
O5	1.004(1)	0.986(1)	0.217(1)	1	0.005(2)	1.005(2)	0.980(2)	0.218(2)	1	0.016(2)
O6	0.043(2)	0.2412(9)	0.261(1)	1	0.005(2)	0.036(2)	0.236(1)	0.269(2)	1	0.016(2)
O7	0.461(1)	0.227(1)	0.273(1)	1	0.005(2)	0.471(2)	0.226(1)	0.278(2)	1	0.016(2)
O8	0.504(1)	0.989(1)	0.222(1)	1	0.005(2)	0.501(2)	0.988(1)	0.220(2)	1	0.016(2)
Ca1	0.7159(6)	0.0772(5)	0.3564(7)	1	0.052(2)	0.7285(9)	0.0824(8)	0.3543(9)	1	0.070(3)
W1	0.254(2)	0.104(1)	0.503(2)	1	0.022(3)	0.259(2)	0.102(2)	0.501(3)	1	0.033(3)
W2	0.591(2)	0.122(2)	0.536(1)	1	0.022(3)	0.592(2)	0.125(2)	0.532(2)	1	0.033(3)
W3	0.911(2)	0.116(2)	0.495(2)	1	0.022(3)	0.910(2)	0.122(2)	0.503(2)	1	0.033(3)
W4	0.777(1)	0.239(5)	0.240(6)	0.38(2)	0.022(3)	0.77(1)	0.274(9)	0.20(1)	0.23(2)	0.033(3)
W5	0.734(3)	0.307(3)	0.410(3)	0.62(2)	0.022(3)	0.745(4)	0.318(3)	0.360(4)	0.77(2)	0.033(3)
W6	0.777(1)	0.083(1)	0.040(1)	0.15(2)	0.022(3)	0.760(6)	0.152(6)	0.06(1)	0.50(9)	0.033(3)
W7	0.760(4)	0.198(3)	0.147(4)	0.62(2)	0.022(3)	0.767(7)	0.175(6)	0.14(1)	0.50(9)	0.033(3)

those reported by Rinaldi and Vezzalini (1985), and the same (Si, Al) ordering in the tetrahedral sites is found (Tables 4 and 5).

The *P*-induced deformation mode of the gismondine framework consists in a slight distortion of the "double crankshaft" chains visible in Figure 1. The same deformation mechanism, even if to a different extent, was observed in gismondine compressed with non-penetrating *P*-transmitting medium (Betti et al. 2007) and in the dehydrated form (Vezzalini et al. 1993).

Figures 4 and 5 show the projections along [100] and [001] at P_{amb}, 1.9 GPa, and P_{amb}(rev) and show the two crystallographically independent 8-membered rings, labeled 8mR-1 and 8mR-2, respectively. Table 7 reports the dimensions of both 8mR-1 and 8mR-2 rings at different pressures for the discussed structures. Notwithstanding the high uncertainties on the reported distances, one can see that, from P_{amb} to 1.9 GPa, both 8mR-1 and 8mR-2 become more elliptical, even if the elongation axes are different. Upon pressure release the channel apertures change, but do not recover their initial geometry (Figs. 4c and 5c; Table 7).

Extraframework species. At ambient conditions the Ca cations are coordinated to all the seven water molecules and to three framework O atoms (O4, O7, O8) belonging to Al2 tetrahedra (Table 6, bond distances <3.2 Å). On the basis of the excessively short W4-W5 distance, the occupancy factors of these partially occupied water sites were constrained to sum 100%. The occupancy factors of the other two partially occupied water sites W6 and W7 progressively increased upon compression, and their sum reached the highest possible value of 100% at 0.6 GPa. Above this pressure, W6 and W7 occupancy factors were constrained to sum 100%. At 0.6 GPa, the total electron number of the O atoms belonging to the water molecules was 160, compared to 152 at P_{amb}, thus highlighting a moderate *P*-induced over-hydration (Fig. 6).

The constrains applied to the two pairs of water sites (W4-W5 and W6-W7) were maintained at pressures up to 1.9 GPa, whereupon a significant water system rearrangement and ordering was observed: the water molecules partially occupying the W4, W5, W6, and W7 sites migrated to fully occupy only two of these positions (W5 and W7), whereas the W4 and W6 sites disappeared (Fig. 7). The *P*-induced re-arrangement of the gismondine water molecule system is summarized in Table 6, where the *P*-dependent reinforcement and the appearance/disappearance of some water-framework interactions can be followed. From Figure 6 and Tables 4 and 6 it is possible to conclude that the over-hydration, but not the water ordering, is substantially irreversible upon pressure release. The only other case of *P*-induced migration and ordering effect in a zeolite water system was reported for the over-hydrated laumontite (Lee et al. 2004b).

Again at 1.9 GPa, O5 approaches the Ca cation, reducing its bond distance from 3.3 Å at P_{amb} to 3.09 Å. The entering of this new framework oxygen into the Ca coordination shell, the previously described water ordering, and the general strengthening of the water-cation bonds, cause a significant re-arrangement also in the Ca coordination polyhedron (Figs. 4 and 5; Table 6). All these changes are reversible upon decompression. From 1.9 up to 2.8 GPa the extra-framework content of monoclinic gismondine did not undergo further substantial modifications.

TABLE 5. T-O framework distances (Å) for monoclinic gismondine at selected pressures

	P_{amb}	1.6 GPa	1.9 GPa	P_{amb}(rev)
Si1-O2	1.622(2)	1.620(4)	1.621(5)	1.631(4)
Si1-O3	1.620(2)	1.619(4)	1.621(4)	1.628(4)
Si1-O7	1.621(2)	1.616(4)	1.620(5)	1.620(4)
Si1-O8	1.621(2)	1.617(4)	1.619(5)	1.623(4)
mean	1.621	1.618	1.620	1.626
Si2-O1	1.618(2)	1.617(4)	1.623(4)	1.627(4)
Si2-O4	1.621(2)	1.617(4)	1.618(4)	1.627(4)
Si2-O5	1.621(2)	1.617(4)	1.623(5)	1.622(4)
Si2-O6	1.621(2)	1.621(4)	1.622(5)	1.621(4)
mean	1.620	1.618	1.622	1.624
Al1-O1	1.738(2)	1.737(4)	1.743(4)	1.749(3)
Al1-O2	1.742(2)	1.748(4)	1.743(5)	1.753(4)
Al1-O5	1.740(2)	1.739(4)	1.743(5)	1.741(4)
Al1-O6	1.741(2)	1.741(4)	1.741(5)	1.738(4)
mean	1.740	1.741	1.743	1.745
Al2-O3	1.739(2)	1.742(4)	1.743(4)	1.749(3)
Al2-O4	1.741(2)	1.743(4)	1.743(5)	1.751(4)
Al2-O7	1.740(2)	1.738(4)	1.744(5)	1.739(4)
Al2-O8	1.741(2)	1.740(4)	1.740(5)	1.742(4)
mean	1.740	1.741	1.743	1.745

TABLE 4—*EXTENDED*

	1.9 GPa					P_{amb}(rev)				
	x/*a*	y/*b*	z/*c*	Occ.	U_{iso}	x/*a*	y/*b*	z/*c*	Occ.	U_{iso}
Si1	0.417(1)	0.108(2)	0.184(1)	1	0.032(2)	0.412(1)	0.108(1)	0.181(1)	1	0.025(2)
Si2	0.909(1)	0.862(2)	0.163(2)	1	0.032(2)	0.909(1)	0.869(1)	0.160(1)	1	0.025(2)
Al1	0.096(1)	0.114(2)	0.170(1)	1	0.032(2)	0.094(1)	0.112(1)	0.166(1)	1	0.025(2)
Al2	0.583(1)	0.860(2)	0.158(1)	1	0.032(2)	0.593(1)	0.866(1)	0.148(1)	1	0.025(2)
O1	0.071(3)	0.164(2)	0.000(1)	1	0.026(3)	0.077(2)	0.168(2)	0.999(1)	1	0.013(2)
O2	0.261(1)	0.071(2)	0.220(2)	1	0.026(3)	0.261(1)	0.062(2)	0.212(2)	1	0.013(2)
O3	0.434(2)	0.139(2)	0.022(1)	1	0.026(3)	0.435(2)	0.157(2)	0.027(1)	1	0.013(2)
O4	0.248(1)	0.397(2)	0.303(2)	1	0.026(3)	0.243(1)	0.406(2)	0.303(2)	1	0.013(2)
O5	1.006(2)	0.978(2)	0.212(2)	1	0.026(3)	1.006(2)	0.982(2)	0.215(2)	1	0.013(2)
O6	0.029(2)	0.233(2)	0.271(2)	1	0.026(3)	0.048(2)	0.244(1)	0.254(2)	1	0.013(2)
O7	0.485(2)	0.225(2)	0.267(2)	1	0.026(3)	0.459(2)	0.231(2)	0.269(2)	1	0.013(2)
O8	0.500(2)	0.985(2)	0.236(2)	1	0.026(3)	0.505(2)	0.988(1)	0.222(2)	1	0.013(2)
Ca1	0.744(1)	0.0777(9)	0.346(1)	1	0.091(4)	0.7164(9)	0.0793(8)	0.356(1)	1	0.071(3)
W1	0.260(3)	0.111(2)	0.497(3)	1	0.038(4)	0.248(3)	0.110(2)	0.502(3)	1	0.035(4)
W2	0.597(3)	0.128(2)	0.519(2)	1	0.038(4)	0.585(2)	0.117(2)	0.552(2)	1	0.035(4)
W3	0.906(3)	0.119(2)	0.514(2)	–	0.038(4)	0.911(2)	0.120(2)	0.492(2)	1	0.035(4)
W4	–	–	–	1		0.802(6)	0.268(6)	0.246(7)	0.44(3)	0.035(4)
W5	0.764(3)	0.303(2)	0.326(3)	–	0.038(4)	0.749(5)	0.294(4)	0.392(6)	0.56(3)	0.035(4)
W6	–	–	–	1		0.754(2)	0.11(1)	0.01(2)	0.16(2)	0.035(4)
W7	0.758(3)	0.149(2)	0.099(2)		0.038(4)	0.750(4)	0.194(4)	0.168(4)	0.79(3)	0.035(4)

TABLE 6. Coordination distances (<3.20 Å) of the extraframework species for selected refinements of monoclinic gismondine

		P_{amb}	1.6 GPa	1.9 GPa	P_{amb}(rev)			P_{amb}	1.6 GPa	1.9 GPa	P_{amb}(rev)
Ca1-	O4	2.48(1)	2.43(2)	2.40(2)	2.46(2)	W4-	O5			–	2.99(6)
	O5			3.09(2)			O6	2.66(5)	2.7(1)	–	2.47(6)
	O7	3.08(1)	3.03(2)	3.07(2)	3.13(2)		O7	3.20(6)	3.1(1)	–	
	O8	2.63(1)	2.75(2)	2.78(2)	2.64(2)		Ca1	2.17(5)	2.57(9)	–	2.45(6)
	W1	2.38(2)	2.41(2)	2.52(2)	2.46(2)		W2	3.05(6)	2.6(1)	–	3.09(6)
	W2	2.26(2)	2.28(2)	2.30(2)	2.41(2)		W3	3.09(6)	2.7(1)	–	3.01(7)
	W3	2.37(2)	2.31(2)	2.29(3)	2.36(2)		W3	3.19(5)		–	3.05(6)
	W4	2.17(5)	2.57(9)	–	2.45(6)		W5	1.89(5)	1.7(1)	–	1.58(7)
	W5	2.50(3)	2.50(3)	2.41(2)	2.33(5)		W6	2.6(1)	1.9(2)	–	2.9(2)
	W6	3.2(1)	3.0(1)	–			W6			–	3.0(2)
	W7	2.47(3)	2.4(1)	2.52(2)	2.26(3)		W7	1.02(6)	1.2(1)	–	1.20(2)
W1-	O1	3.11(2)	3.13(3)	3.03(2)	2.92(3)	W5-	O2	3.03(3)	2.80(3)	2.86(3)	3.03(4)
	O2	2.85(2)	2.75(3)	2.73(4)	2.90(3)		O5		3.13(4)	2.95(3)	
	O3	3.17(2)	3.16(3)	3.16(3)	3.10(3)		O6		3.16(4)	2.76(3)	
	O4	2.95(2)	2.91(3)	2.97(3)	2.96(3)		O7	3.11(3)	2.96(4)	2.90(3)	3.17(5)
	Ca1	2.38(2)	2.41(2)	2.52(2)	2.46(2)		O8		3.11(4)		
	W2	2.89(2)	2.85(2)	2.90(3)	2.99(3)		Ca1	2.50(3)	2.50(3)	2.41(2)	2.33(5)
	W3	2.86(2)	2.90(3)	2.94(3)	2.92(3)		W2	2.75(3)	3.07(4)	3.13(3)	2.99(5)
							W3	2.80(3)	2.96(4)	2.99(3)	2.63(4)
W2-	O3	2.87(2)	2.83(3)	2.95(3)	2.85(3)		W4	1.89(5)	1.7(1)	–	1.58(7)
	O7	3.05(2)	2.91(3)	2.86(3)	3.00(3)		W6	1.8(1)	2.0(1)	–	1.6(2)
	O7	3.15(2)	3.15(3)	3.09(3)			W7	2.85(4)	2.7(1)	2.69(3)	2.45(6)
	O8	2.85(2)	2.89(2)	2.84(3)	2.67(3)		W7	2.34(3)	2.7(1)	2.74(2)	2.71(6)
	Ca1	2.26(2)	2.28(2)	2.30(2)	2.41(2)						
	W1	2.89(2)	2.85(2)	2.90(3)	2.99(3)	W6-	O1	3.1(1)	3.16(7)	–	
	W3		3.17(2)	3.03(3)			O1	3.0(1)		–	
	W4	3.05(6)	2.6(1)	–	3.09(6)		O2	3.0(1)		–	2.9(2)
	W5	2.75(3)	3.07(4)	3.13(3)	2.99(5)		O3		3.20(6)	–	
	W6		2.88(6)	–			O4	2.5(1)	2.99(7)	–	2.8(2)
	W7	2.74(4)	2.90(6)	2.94(3)	2.81(4)		O5	3.0(1)		–	
							Ca1	3.2(1)	3.0(1)	–	
W3-	O1	2.88(2)	2.81(3)	2.82(3)	2.80(3)		W2		2.88(6)	–	
	O5	3.12(2)	3.02(2)	2.97(3)	3.16(2)		W3		2.88(6)	–	
	O6	3.01(2)	2.90(3)	2.93(3)	3.06(3)		W4	2.6(1)	1.9(2)	–	2.9(2)
	O6			3.17(3)			W4			–	3.0(2)
	Ca1	2.37(2)	2.31(2)	2.29(3)	2.36(2)		W5	1.8(1)	1.9(1)	–	1.6(2)
	W1	2.86(2)	2.90(3)	2.94(3)	2.92(3)		W7	1.6(1)	0.82(7)	–	1.8(2)
	W2		3.17(2)	3.03(3)							
	W3	3.03(3)	3.13(4)	3.14(4)	3.10(4)	W7-	O4	3.18(4)	2.94(6)	2.85(3)	3.08(4)
	W4	3.09(6)	2.7(1)	–	3.01(7)		O5		3.20(6)		
	W4	3.19(5)		–	3.05(6)		O6	3.05(4)	3.0(1)		3.11(4)
	W5	2.80(3)	2.96(4)	2.99(3)	2.63(4)		O7				3.15(4)
	W6		2.88(6)	–			Ca1	2.47(3)	2.4(1)	2.52(2)	2.26(3)
	W7	2.94(3)	2.92(6)	2.98(3)	3.12(4)		W2	2.74(4)	2.90(6)	2.94(3)	2.81(4)
							W3	2.94(3)	2.92(6)	2.98(3)	3.12(4)
							W4	1.02(6)	1.2(1)	–	1.02(7)
							W5	2.85(4)	2.7(1)	2.69(3)	2.45(6)
							W5	2.34(3)	2.7(1)	2.74(2)	2.71(6)
							W6	1.6(1)	0.82(7)	–	1.8(2)

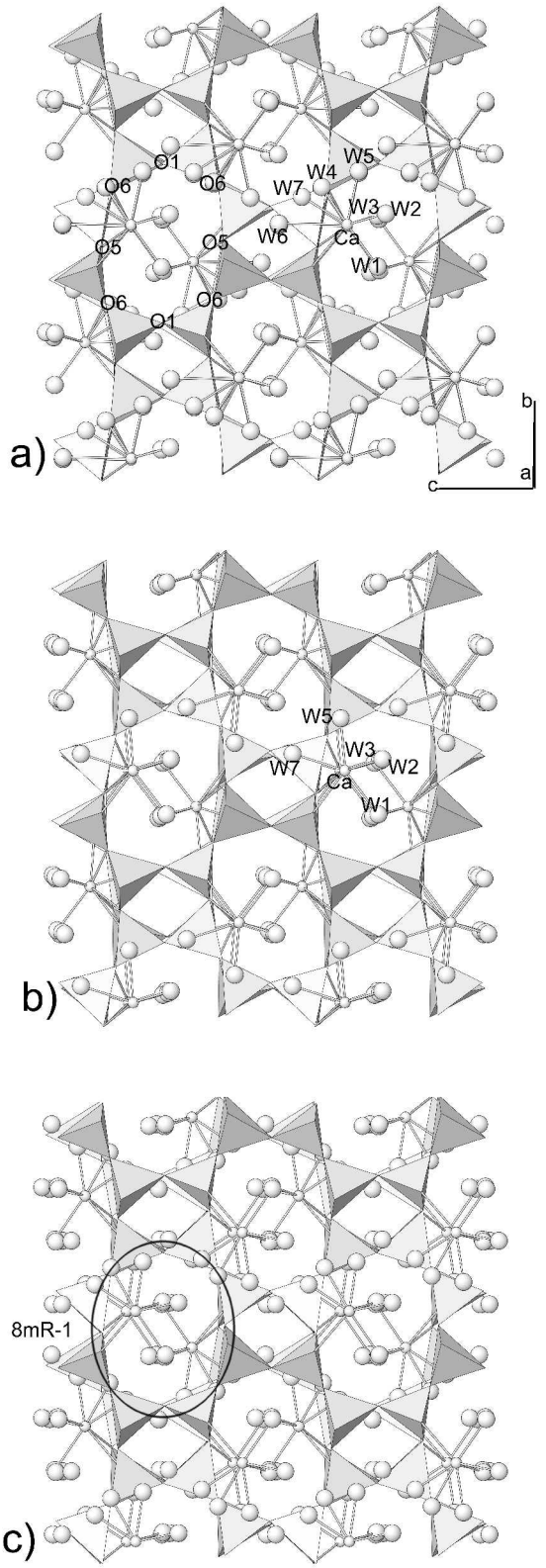

FIGURE 4. Projection of the gismondine structure along the [100] direction at **(a)** P_{amb}, **(b)** 1.9 GPa, and **(c)** P_{amb}(rev).

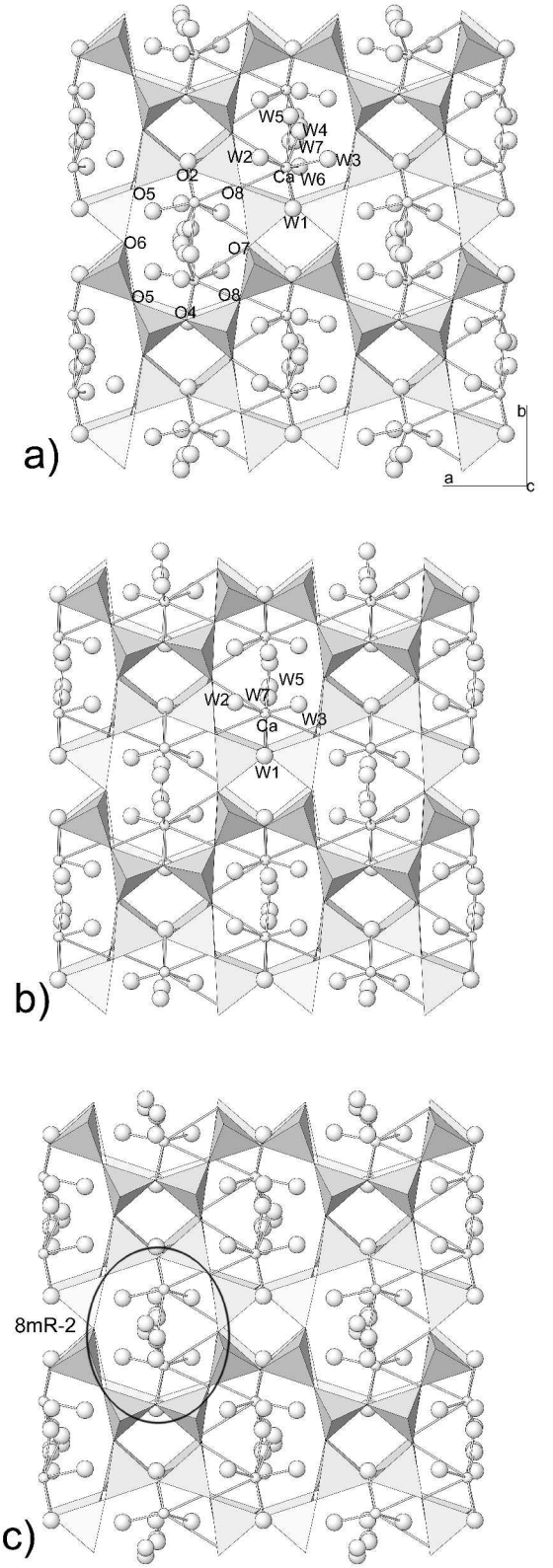

FIGURE 5. Projection of the gismondine structure along the [001] direction at **(a)** P_{amb}, **(b)** 1.9 GPa, and **(c)** P_{amb}(rev).

TABLE 7. Internal diameters (Å) of the two independent 8-membered rings present in the monoclinic gismondine structure at selected pressures

	P_{amb}	1.6 GPa	1.9 GPa	P_{amb}(rev)
	8mR-1 [Si1-Al1-Si2-Si1-Al2-Si1-Al2-Al1]			
O1-O1	7.38(3)	7.35(4)	7.28(4)	7.22(3)
O6-O6	7.02(3)	6.78(3)	6.69(4)	7.18(4)
O6-O6	7.54(3)	7.69(3)	7.74(4)	7.41(4)
O5-O5	5.58(3)	5.53(4)	5.62(4)	5.63(4)
	8mR-2 [Al1-Si1-Al2-Si1-Al2-Si2-Al1-Si2]			
O2-O4	7.12(1)	7.12(2)	7.20(2)	7.03(2)
O5-O8	7.23(2)	7.16(2)	7.14(3)	7.19(2)
O8-O5	7.41(2)	7.39(2)	7.35(3)	7.46(2)
O6-O7	5.84(1)	5.59(2)	5.33(2)	5.91(2)

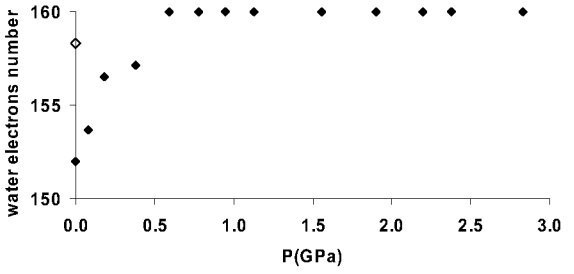

FIGURE 6. Total number of electrons of the water O atoms ("water electron number") in monoclinic gismondine as a function of pressure; empty symbol stands for total water electrons at P_{amb} after decompression.

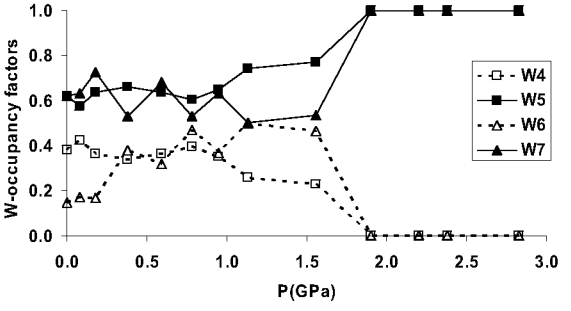

FIGURE 7. Occupancy factors for the partially occupied water sites (W4, W5, W6, W7) at increasing pressures.

Structural interpretation of the evolution of the lattice parameters. The *P*-induced evolution of the unit-cell constants of monoclinic gismondine and the discontinuity at about 2 GPa can be rationalized on the basis of the framework and extra-framework modifications. The *a* and *c* axes undergo a larger compression (about –2.9 and –1.8%, respectively) than does the *b* axis, which is even slightly elongated (+0.1%) at the highest pressure of the stability field of monoclinic gismondine. This behavior can be interpreted considering that *a* and *c* are the directions along which the highly deformable "double crankshaft" chains extend (Fig. 1). These chains slightly increase their zigzag behavior upon compression, so favoring *a* and *c* contractions. The higher compressibility of gismondine along [100] with respect to [001] could otherwise be related to the preponderance of the Ca-O_{frame} bonds in the former direction (Figs. 4 and 5). The abrupt volume decrease, occurring at 1.9 GPa, can be attributed to the water migration and associated decrease of the occupied water sites. In this way, the larger free volume available in the cavities allows an easier framework contraction.

Some specific consideration must be given to the evidence that, in gismondine, PIH and *P*-induced water ordering occur without any cell-volume expansion. The anomalous increase of cell volume under compression has up to now been considered as a concomitant event, necessarily accompanying the PIH phenomenon (see for example the recent paper by Likhacheva et al. 2007 and the literature there cited). However, in zeolites characterized by the presence of partially occupied water sites (like gismondine) the penetration of additional water might only result in an increased site occupancy, rather than in the appearance of new extraframework sites, and hence it might occur without volume expansion.

BULK MODULUS CALCULATION

In the previous sections we have interpreted, from the structural point of view, the deformation mechanism and the over-hydration/water-ordering phenomena observed in gismondine compressed in m.e.w. These complex phenomena have a large effect on the unit-cell parameters, which clearly show several discontinuities. Now, on the basis of the results of the structural analyses, the interpretation of these discontinuities can be applied to the calculation of the bulk modulus.

In particular, the region of very low pressure (between P_{amb} and 0.6 GPa) must be excluded by the calculation of the bulk modulus because the over-hydration effect gives rise to a continuous change of the chemistry of the system; at 0.6 GPa the over-hydration process is complete, and the chemistry is constant up to the maximum *P* achieved (Fig. 6). In addition, in the *P* range 4.3–5.7 GPa, the *P*-dependence of the cell axes, angles, and volume undergo at least two slope variations at different *P* values for each set of parameters, suggesting that, in this region, triclinic gismondine is in a metastable state. As a consequence, also this *P* range was excluded in the volume bulk modulus calculation, and hence the following four pressure ranges were considered: 0.6–1.6, 1.9–2.8, 3.3–4.0, and 6.5–7.9 GPa. Due to the low number of experimental observations and the restricted *P* ranges of the four baric regions, no equations of state were able to correctly fit the experimental data. As a consequence, the volume bulk modula were calculated with the following procedure: V_0 values were obtained by extrapolating the experimental data with a linear regression; then, the compressibility in each *P* range was determined as the slope of the V/V_0 vs. *P* curve. The following values were obtained for the four *P* ranges, respectively: V_0 = 1044 (1) Å^3, K_0 = 69(5) GPa; V_0 = 1036(5) Å^3, K_0 = 74 (9) GPa; V_0 = 1034(7) Å^3, K_0 = 75 (9) GPa; and V_0 = 1134(6) Å^3, K_0 = 61(5) GPa.

Comparison between gismondine compressibility in aqueous medium and silicone oil

It is interesting to compare the compressibility behaviors and the *P*-induced structural deformations of gismondine here investigated in m.e.w., a nominally penetrating *P*-transmitting medium, and in s.o., a non-penetrating one (Betti et al. 2007). In both cases, no complete amorphization is observed in the studied *P* range. Moreover, the original lattice parameters, but not the

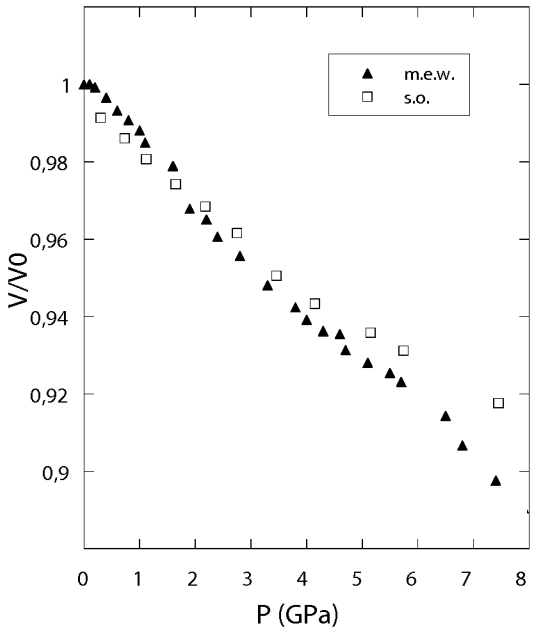

FIGURE 8. Comparison of the unit-cell volume variations as a function of pressure for gismondine compressed in in m.e.w. (triangles, this work) and s.o. (squares, Betti et al. 2007).

structural details, are substantially recovered upon decompression. The bulk modulus values determined for gismondine in both experiments are among the highest found up to now for zeolites, confirming the low-compressibility behavior of this zeolite, which, on the contrary, is extremely flexible upon dehydration (Vezzalini et al. 1993). On the basis of the structural refinements of monoclinic gismondine, we note that the framework deformation mechanism is the same deduced by the molecular dynamics simulations performed by Betti et al. (2007), that is, basically driven by the distortion of the "double crankshaft" chains. In both experiments, the *P*-induced deformations also give rise to a rearrangement in the Ca polyhedron.

Some significant differences can, on the other hand, be singled out from the two experiments. Notwithstanding that both studies suggest the tendency of the gismondine unit cell toward tetragonality upon compression, for gismondine in m.e.w., a transition to a triclinic phase is observed at about 3 GPa, whereas gismondine compressed in s.o. remains monoclinic up to 7.4 GPa, and only at this pressure some new non-indexable peaks appear, suggesting the possible onset of a phase transition.

More important, the gismondine unit-cell volume decreases by about 11 and 8% in m.e.w. and s.o., respectively (Fig. 8). This is a novel result in the studies of zeolite compressibility behavior. In fact, up to now, all the zeolites compressed with both aqueous penetrating medium (and subject to PIH effect) and non-penetrating one, showed a much lower compressibility under the first condition (see Table 4 in Colligan et al. 2004; Likhacheva et al. 2006, 2007), due to the ability of the aqueous medium to penetrate the pores and channels of the framework. Silicone oil cannot penetrate, therefore all pressure exerted on the sample goes directly into compression of the framework and leads to a lower bulk modulus.

To compare in more detail the elastic behavior of gismondine in the two different *P*-transmitting media, we have re-calculated the bulk modulus in s.o. using the data by Betti et al. (2007), considering two distinct *P* ranges (0.4–2.8 and 4.7–7.4 GPa) and adopting the same procedure used in this work for gismondine in m.e.w. The corresponding elastic parameters are $V_0 = 1051.8(5)$, $K_0 = 80(2)$ and $V_0 = 1031.3(5)$, $K_0 = 125(1)$, respectively. The much lower K_0 of gismondine in m.e.w. with respect to s.o.—in particular in the highest *P* regime [$K_0 = 61(5)$ GPa]—is ascribable to the previously discussed re-organization of the water molecules, which leaves a larger free volume inside the pores and hence allows a higher compressibility in the penetrating aqueous medium. The over-hydration and the water-ordering phenomena could also be responsible for the early monoclinic-triclinic phase transition undergone by gismondine in m.e.w.

ACKNOWLEDGMENTS

This work was supported by the Italian MIUR (PRIN2006 "Zeolites at non-ambient conditions: Theoretical-experimental characterization and novel technological applications"). The Swiss-Norwegian beamline (BM01) at European Synchrotron Radiation Facility is acknowledged for allocation of beamtime and for technical support during the experiments. The authors thank Y. Lee for some preliminary compression tests performed on gismondine at NSLS. G. Diego Gatta, an anonymous referee, and Martin Kunz are acknowledged for the constructive suggestions and comments, which contributed to improve the manuscript.

REFERENCES CITED

Adams, C.J., Araya, A., Carr, S.W., Chapple, A.P., Franklin, K.R., Graham, P., Minihan, A.R., Osinga, T.J., and Stuart, J.A. (1997) Zeolite map: The new detergent zeolite. Studies Surface Science and Catalysis, 105B, 1667–1674.

Artioli, G., Rinaldi, R., Kvick, A., and Smith, J.V. (1986) Neutron diffraction structure refinement of the zeolite gismondine at 15 K. Zeolites, 6, 361–366.

Baerlocher, Ch., Meier, W.M., and Olson, D.H. (2001) Atlas of zeolite framework types. Elsevier, Amsterdam.

Betti, C., Fois, E., Mazzuccato, E., Medici, C., Quartieri, S., Tabacchi, G., Vezzalini, G., and Dmitriev, V. (2007). Gismondine under HP: Deformation mechanism and re-organization of the extra-framework species. Microporous and Mesoporous Materials, 103, 190–209.

Colligan, M., Foster, P.M., Cheetman, A.K., Lee, Y., Vogt, T., and Hriljac, J.A. (2004) Synchrotron X-ray powder diffraction and computational investigation of purely siliceus zeolite Y under pressure. Journal of American Chemical Society, 126, 12015–12022.

Colligan, M., Lee, Y., Vogt, T., Celestian, A.J., Parise, J.B., Marshall, W.G., and Hriljac, J.A. (2005) High-pressure neutron diffraction study of superhydrated natrolite. Journal of Physical Chemistry B, 109, 18223–18225.

Cromer, D.T. and Waber, J.R. (1974) Atomic scattering factors for X-rays. International Tables for X-ray Crystallography, vol. IV, Section 2.2, p. 99–101. Kynoch Press, Birmingham, U.K.

Fischer, K. and Schramm, V. (1971) Crystal structure of gismondine, a detailed refinement. American Chemical Society, Advances in Chemistry Series, 101, 508–516.

Forman, R.A., Piermarini, G.J., Barnett, J.D., and Block, S. (1972) Pressure measurements made by utilization of the ruby sharp-line luminescence. Science, 176, 284–286.

Gatta, G.D. and Lee, Y. (2006) On the elastic behavior of zeolite mordenite: A synchrotron powder diffraction study. Physics and Chemistry of Minerals, 32, 726–732

Gatta, G.D., Boffa Ballaran, T., Comodi, P., and Zanazzi, P.F. (2004a) Isothermal equation of state and compressional behavior of tetragonal edingtonite. American Mineralogy, 89, 633–639.

——— (2004b) Comparative compressibility and equation of state of orthorhombic and tetragonal edingtonite. Physics and Chemistry of Minerals, 31, 288–298

Gatta, G.D., Nestola, F., and Boffa Ballaran, T. (2006) Elastic behavior, phase transition, and pressure induced structural evolution of analcime. American Mineralogist, 91, 568–578.

Håkansson, U., Fälth, L., and Hansen, S. (1990) Structure of a high-silica variety of zeolite Na-P. Acta Crystallographica, C46, 1363–1364.

Hammersley, A.P., Svensson, S.O., Hanfland, M., Fitch, A.N., and Häusermann, D. (1996) Two-dimensional detector software: From real detector to idealized image or two-theta scan. High Pressure Research, 14, 235–248.

Hazen, R.M. (1983) Zeolite molecular sieve 4A: Anomalous compressibility and volume discontinuities at high pressure. Science, 219, 1065–1067.

Hazen, R.M. and Finger, L.W. (1984) Compressibility of zeolite 4A is dependent on the molecular size of the hydrostatic pressure medium. Journal of Applied

Physics, 56, 1838–1840.
Larson, A.C. and Von Dreele, R.B. (1996) GSAS—general structure analysis system. Report LAUR 86-748, Los Alamos National Laboratory, New Mexico.
Le Bail, A., Duroy, H., and Fourquet, J.L. (1988) Ab-initio structure determination of $LiSbWO_6$ by X-ray powder diffraction. Material Research Bulletin, 23, 447–452.
Lee, Y., Hriljac, J.A., Vogt, T., Parise, J.B., and Artioli, G. (2001a) First structural investigation of a super-hydrated zeolite. Journal of the American Chemical Society, 123, 12732–12733.
Lee, Y., Hriljac, J.A., Vogt, T., Parise, J.B., Edmondson, M.J., Anderson, P.A., Corbin, D.R., and Takaya, N. (2001b) Phase transition of zeolite RHO at high-pressure. Journal of American Chemical Society, 123, 8418–8419.
Lee, Y., Vogt, T., Hriljac, J.A., Parise, J.B., and Artioli, G. (2002a) Pressure-induced volume expansion of zeolites in the natrolite family. Journal of American Chemical Society, 124, 5466–5475.
Lee, Y., Vogt, T., Hriljac, J.A., Parise, J.B., Hanson, J.C., and Kim, S.J. (2002b) Non-framework cation migration and irreversible pressure-induced hydration in a zeolite. Nature, 420, 485–489.
Lee, Y., Hriljac, J.A., Studer, A., and Vogt, T. (2004a) Anisotropic compression of edingtonite and thomsonite to 6 GPa at room temperature. Physics and Chemistry of Minerals, 31, 22–27.
Lee, Y., Hriljac, J.A., and Vogt, T. (2004b) Pressure-induced migration of zeolitic water in laumontite. Physics and Chemistry of Minerals, 31, 421–428.
Lee, Y., Hriljac, J.A., Parise, J.B., and Vogt, T. (2006) Pressure-induced hydration in zeolite tetranatrolite. American Mineralogist, 91, 247–251.
Likhacheva, A.Yu., Seryotkin, Y.V., Manakov, A.Yu., Goryainov, S.V., Ancharov, A.I., and Sheromov, M.A. (2006) Anomalous compression of scolecite and thomsonite in aqueous medium to 2 GPa. High Pressure Research, 26, 449–453.
——— (2007) Pressure-induced over-hydration of thomsonite: A synchrotron powder diffraction study. American Mineralogist, 92, 1610–1615.
Mao, H.K., Xu, J., and Bell, P.M. (1986) Calibration of the ruby pressure gauge to 800 kbar under quasi-hydrostatic conditions. Journal of Geophysical Research, 91, 4673–4676.
Miletich, R., Allan, D.R., and Kush, W.F. (2000) High-pressure single-crystal techniques. In R.M. Hazen and R.T. Downs, Eds., High-temperature and High-pressure Crystal Chemistry, 41, p. 445–519. Reviews in Mineralogy and Geochemistry, Mineralogical Society of America, Chantilly, Virginia.
Ori, S. (2008) Structural modifications of zeolites at non ambient conditions. Ph.D. thesis, University of Modena and Reggio Emilia.
Rinaldi, R. and Vezzalini, G. (1985) Gismondine: the detailed X-ray structure refinement of two natural samples. In B. Drzaj, S. Hocevar, and S. Pejovnik, Eds., Zeolites synthesis, structure, technology and application. Studies in Surface Science and Catalysis, 24, 481–492.
Seryotkin, Yu.V., Bakakin, V.V., Fursenko, B.A., Belitsky, I.A., Joswig, W., and Radaelli, P.G. (2005) Structural evolution of natrolite during over-hydration: A high-pressure neutron diffraction study. European Journal of Mineralogy, 17, 305–313.
Thomson, P., Cox, D.E., and Hastings, J.B. (1987) Rietveld refinement of Debye-Scherrer synchrotron X-ray data from Al_2O_3. Journal of Applied Crystallography, 20, 79–83.
Toby, B.H. (2001) EXPGUI, a graphical user interface for GSAS. Journal of Applied Crystallography, 34, 210–213.
Vezzalini, G. and Oberti, R. (1984) The crystal chemistry of gismondines. Bulletin de Minéralogie, 107, 805–812.
Vezzalini, G., Quartieri, S., and Alberti, A. (1993) Structural modifications induced by dehydration in the zeolite gismondine. Zeolites, 13, 34–42.
Werner, P.E., Eriksson, L., and Westdhal, M. (1985) TREOR, a semi-exhaustive trial-and-error powder indexing program for all symmetries. Journal of Applied Crystallography, 18, 367–370.

MANUSCRIPT RECEIVED OCTOBER 25, 2007
MANUSCRIPT ACCEPTED FEBRUARY 15, 2008
MANUSCRIPT HANDLED BY MARTIN KUNZ